PNAS RESEARCH ARTICLE | CELL BIOLOGY OPEN ACCESS

Superresolution microscopy localizes endogenous Dvl2 to Wnt signaling-responsive biomolecular condensates

Antonia Schubert[a,b,c], Oksana Voloshanenko[a], Franziska Ragaller[a,1], Philipp Gmach[a,2], Dominique Kranz[a], Christian Scheeder[a], Thilo Miersch[a], Matthias Schulz[b], Lorenz Trümper[b], Claudia Binder[b], Marko Lampe[d], Ulrike Engel[e], and Michael Boutros[a,3]

Edited by Roel Nusse, Stanford University School of Medicine, Stanford, CA; received December 13, 2021; accepted April 15, 2022

During organismal development, homeostasis, and disease, Dishevelled (Dvl) proteins act as key signaling factors in beta-catenin–dependent and beta-catenin–independent Wnt pathways. While their importance for signal transmission has been genetically demonstrated in many organisms, our mechanistic understanding is still limited. Previous studies using overexpressed proteins showed Dvl localization to large, punctate-like cytoplasmic structures that are dependent on its DIX domain. To study Dvl's role in Wnt signaling, we genome engineered an endogenously expressed Dvl2 protein tagged with an mEos3.2 fluorescent protein for superresolution imaging. First, we demonstrate the functionality and specificity of the fusion protein in beta-catenin–dependent and beta-catenin–independent signaling using multiple independent assays. We performed live-cell imaging of Dvl2 to analyze the dynamic formation of the supramolecular cytoplasmic Dvl2_mEos3.2 condensates. While overexpression of Dvl2_mEos3.2 mimics the previously reported formation of abundant large "puncta," supramolecular condensate formation at physiological protein levels is only observed in a subset of cells with approximately one per cell. We show that, in these condensates, Dvl2 colocalizes with Wnt pathway components at gamma-tubulin and CEP164-positive centrosomal structures and that the localization of Dvl2 to these condensates is Wnt dependent. Single-molecule localization microscopy using photoactivated localization microscopy (PALM) of mEos3.2 in combination with DNA-PAINT demonstrates the organization and repetitive patterns of these condensates in a cell cycle–dependent manner. Our results indicate that the localization of Dvl2 in supramolecular condensates is coordinated dynamically and dependent on cell state and Wnt signaling levels. Our study highlights the formation of endogenous and physiologically regulated biomolecular condensates in the Wnt pathways at single-molecule resolution.

Wnt signaling | Dishevelled | superresolution microscopy | biomolecular condensates | CRISPR

Significance

Wnt signaling governs cell fate and tissue polarity across species. The Dishevelled proteins are central to Wnt signaling cascades. Wnt-mediated multiprotein complexes such as the "signalosome" and the "destruction complex" have been proposed to represent biomolecular condensates. These nonmembranous, specialized compartments have been suggested to form through liquid–liquid phase separation and ensure correctly proceeding physiological reactions. Although biomolecular condensates have increasingly been studied, key questions remain regarding, for example, their architecture and physiological regulation. Here, superresolution microscopy after endogenous labeling of Dishevelled-2 gives insights into protein functions and Wnt signaling at physiological levels. It reveals the distinct molecular architecture of endogenous Wnt condensates at single-molecule resolution and illustrates close interactions at the centrosome.

During development, Wnt signaling drives fundamental cellular processes, such as progenitor cell proliferation, cell fate specification, asymmetric cell division, planar cell polarity, and cell migration (1–3). In the adult tissue and during aging, Wnt signaling controls tissue maintenance, stem cell renewal, and cell proliferation (1–3). The Dishevelled (Dvl) proteins act as crucial signaling integration hubs at the crossroads of beta-catenin–dependent and beta-catenin–independent Wnt signaling pathways, mediating different biological outcomes (4–8). Over the past few decades, the function of Dvl proteins has been widely investigated in different organisms (4, 5, 9, 10).

The three Dvl-paralogues (Dvl1, Dvl2, and Dvl3) in vertebrates are highly conserved in primary sequence and all encode for evolutionarily conserved DIX, PDZ, and DEP domains (4). The N-terminal DIX (Dvl and Axin) domain mediates the formation of homooligomers or heterooligomers and the binding to Axin1 to inhibit the "destruction complex" (4, 11–14). PDZ (Postsynaptic density, Disk large, Zonula occludens-1) is a central domain for both beta-catenin–dependent and beta-catenin–independent signaling and mediates interactions with other PDZ domains and C-terminal ends of membrane receptors (5, 15–17). The C-terminal DEP (Dvl, Egl-10, Pleckstrin) domain stabilizes PDZ-mediated binding to Fzd receptors (18–21).

In the current model, binding of a "canonical" Wnt ligand, such as Wnt3a, to an Fzd receptor leads to the recruitment of an LRP (low-density lipoprotein receptor [LDLR]-related protein) coreceptor (22, 23). Subsequently, Dvl is recruited to the plasma membrane and phosphorylated by the casein kinase 1 (CK1) (22, 24, 25). Dvl then forms oligomers through association via its DIX domain and domain swapping of DEP domains (26, 27). These phosphorylated and activated Dvl polymers can bind to self-associated Axin (26, 28). Binding of Axin then inactivates the cytosolic beta-catenin "destruction complex" of APC (adenomatous polyposis coli), Axin, GSK3-beta, and CK1alpha. Stabilized beta-catenin accumulates in the cytosol and translocates into

This article is a PNAS Direct Submission.

[1]Present address: Science for Life Laboratory, Department of Women's and Children's Health, Karolinska Institutet, 17165 Solna, Sweden.

[2]Present address: Department for Cardiovascular and Metabolic Diseases, Max Delbrück Center for Molecular Medicine in the Helmholtz Association, 13125 Berlin, Germany.

[3]To whom correspondence may be addressed. Email: m.boutros@dkfz.de.

This article contains supporting information online at http://www.pnas.org/lookup/suppl/doi:10.1073/pnas.2122476119/-/DCSupplemental.

Published July 22, 2022.

the nucleus. In the nucleus, it induces the transcription of Wnt target genes through the transcription factors T-cell factor (TCF) and lymphoid enhancer factor (LEF) (as reviewed in ref. 1). Dvl oligomerization and association with other signaling components such as Axin can be induced by overexpression of Dvl, Axin (11, 14, 29–31), and, most likely, also other components such as various kinases (28). These accumulations have previously been described as Dvl "puncta."

While Dvl "puncta" were primarily thought to be associated with vesicular membranes (13), it was later shown that these large structures are actually membraneless protein accumulations dynamically changing and growing through fusion (14). The physiological role of these Dvl "puncta" has been widely discussed. Smalley et al. (29) demonstrated a concentration-dependent formation of ectopically expressed Dvl2 "puncta." As Wnt signaling was already observed at lower expression levels of Dvl2 where no "puncta" formed, it was concluded that Dvl2 "puncta" are protein aggregates not required for Wnt signaling (29). Schwarz-Romond et al. (14, 28, 32) highlighted, in various studies, that the recruitment of Dvl into these dynamic protein accumulations depends on its concentration and the Dvl DIX domain, concluding that their formation is critical for Wnt-dependent Dvl2 signaling. "Signalosomes" describe multimeric, intracellular complexes of activated receptors and associated signaling factors such as Dvl (23, 33), and they play an important role in signaling activation (23, 33).

Biomolecular condensates, a class of nonmembranous organelles, represent specialized compartments of cells, which ensure the correct proceedings of physiological reactions (34). They form dynamically, for example, by phase separation of proteins, biopolymers, and RNA in cells (liquid–liquid phase separation [LLPS]). Free exchange of molecules takes place within the structures and in exchange with their surroundings. They can be up to several micrometers in size (34, 35). Clustering of polymers through modular domains or weak interactions conferred by intrinsically disordered regions (IDRs) leads to the formation of the biomolecular condensates, which locally increases the concentration of the assembling as well as additionally recruited components facilitating biochemical processes (34, 36). The Flory–Huggins theory is a lattice model explaining the thermodynamics of mixing polymers within a solvent (37). It is often applied to explain biomolecular condensate formation. The separation of polymer-rich and polymer-poor phases depends on the net attraction between polymers, determined by concentrations and affinities. Therefore, moderate contextual alterations might induce drastic changes in phase-separated systems (38–40).

"Signalosomes" and the "destruction complex" have recently been suggested to represent biomolecular condensates (35, 41–43). The scaffold protein Axin has been shown to drive the formation of the "destruction complex" through "puncta" formation by self-polymerization mediated through its DAX (Axin DIX) domain (35, 44, 45). Due to Axin's IDRs, which undergo phase separation in vitro, its multivalency, and the fact that Axin "puncta" formation has been observed in living cells, it was proposed that Axin "puncta" represent biomolecular condensates and that Axin is the key organizer of the "destruction complex" by undergoing LLPS (35, 43). Also, APC contains IDRs, which harbor multiple beta-catenin and Axin binding sites and undergo LLPS in vitro (42). Dvl as a multidomain and multivalent protein has been shown to interact with a multitude of other proteins (35, 46). It has been suggested to undergo LLPS; nevertheless, no experimental evidence exists so far (35, 46). Demonstrating the formation of "puncta" or "signalosomes" at endogenous levels was challenging and limited by the lack of suitable antibodies and, possibly, fixation artifacts. Therefore, the existence and requirement of supramolecular Dvl condensates at endogenous protein levels has been questioned.

Genome engineering through CRISPR/Cas-based methods allows overcoming of potential overexpression artifacts mediated by unphysiological protein levels and regulation, by introducing fluorescent tags in the endogenous locus. It has been used to fluorescently label beta-catenin and revisit its role in Wnt signaling (47, 48).

Recently, two endogenous knock-ins with fluorescent labeling of Dvl proteins were published (27, 49). Kan et al. (27) established a C-terminal GFP fusion in HEK293T cells and live-cell fluorescent imaging showed the presence of one or two apparently stable "puncta" in 20% of the cells, but they could not detect the formation of Wnt-dependent Dvl "puncta" (27). Ma et al. (49) created a C-terminally tagged DVL2_mEGFP knock-in. After Wnt3a stimulation, they also observed Dvl2 mostly evenly distributed and rarely in the nucleus or on the membrane in HEK293T cells. Both groups did not further focus on the observed large "puncta" structures in their studies but characterized the behavior of Dvl at the plasma membrane using total internal reflection fluorescence (TIRF) (27, 49).

A number of compelling questions therefore remained: Do Wnt signaling components form large "puncta" at endogenous protein levels? Is their presence relevant for active Wnt signaling? Which proteins colocalize herein, and with which cellular structures are they associated? And, as reviewed in refs. 35 and 46, how do suggested biomolecular condensates such as the "destruction complex" and "signalosomes" communicate with each other?

To answer these questions, we established and characterized an endogenous knock-in of the mEos3.2 fluorophore at the C terminus of *DVL2* in HEK293T cells (HEK293T^{DVL2_mEos}). We show that Dvl2 at endogenous protein levels forms "puncta" that mimic the behavior of biomolecular condensates. Dvl2_mEos3.2 dynamically localizes to non-membrane-bound, supramolecular condensates at the centrosome together with other Wnt signaling components in a Wnt- and cell cycle–dependent manner. However, endogenous condensates are far more scarce and limited to a subset of cells, unlike previously reported "puncta" or "signalosomes." We use single-molecule localization microscopy (SMLM) to analyze the composition of these supramolecular structures.PALM (photoactivated localization microscopy) as a type of SMLM uses fluorophores, such as mEos3.2, that can be converted by irradiation with UV light to reach single-molecule resolution (50, 51). To date, only a few studies have combined CRISPR/Cas9-mediated genome editing with superresolution microscopy, and only a limited number of studies used PALM after endogenously integrating a photoconverting tag in mammalian cells (CRISPR PALM) (52–54). Endogenous labeling allows us to conquer the limitations of classical approaches in cell biology, such as overexpression experiments, and provide unique insights into the physiological behavior and molecular architecture of cell cycle and context-regulated Dvl2 supramolecular condensates in HEK293T cells.

Results

Generation of an Endogenously Tagged Dvl2_mEos3.2 HEK293T Cell Line. To analyze the physiological behavior of Dvl, we used homology-directed repair after CRISPR/Cas9-induced double-strand break formation to fuse the mEos3.2 fluorophore to the *DVL2* C terminus in HEK293T cells (Fig. 1*A* and *SI Appendix*, Fig. S1). We chose mEos3.2 since it is a monomeric, bright, and

fast-maturing photoconvertible fluorophore. Upon near-UV irradiation, it changes from a green to red fluorescent form which allows for superresolution microscopy (PALM) (55, 56). HEK293T cells are a well-characterized and established system to study Wnt signaling responses (6, 57–61), facilitating tests for preserved functionality. We fluorescently labeled the Dvl2 paralog, since it is the most abundant in HEK293T cells, and only weak Dvl3 and no Dvl1 expression can be detected (*SI Appendix*, Fig. S2*A* and ref. 62).

We successfully generated a homozygous and heterozygous knock-in at the *DVL2* locus in clones 142_1 and 142_3, respectively, as confirmed by PCR and gel electrophoresis (Fig. 1*B*). Clone 225 represents a fluorescent clone with incorrect integration of the fluorophore, since no noticeable size shift can be seen after gel electrophoresis of the PCR product (Fig. 1*B*). Western blotting for protein expression analysis and Sanger sequencing revealed that the homozygous knock-in 142_1 clone had a single point mutation, leading to a faulty protein product. Sequencing the heterozygous knock-in 142_3 clone showed correct integration of the fluorophore's sequence (*SI Appendix*, Fig. S1), and the expressed protein showed the expected size of a Dvl2_mEos3.2 fusion protein (about 105 kDa) (Fig. 1*C*). The small interfering RNA (siRNA)–mediated knockdown of *DVL2* confirmed the specific integration of the fluorophore (Fig. 1*C*). CRISPR/Cas9-mediated knockout of all Dvl-paralogs (DVL1,2,3^{KO}) was performed in the HEK293T^{DVL2_mEos} cell line as previously reported (57). Western blot (*SI Appendix*, Fig. S2*B*) and confocal microscopy (*SI Appendix*, Fig. S2*C*) showed loss of the mEos3.2 signals, confirming Dvl specificity. Therefore, the heterozygous clone 142_3 was used for further analysis.

Characterization of Dvl2_mEos3.2 Condensates in HEK293T Cells. It was previously reported that overexpressed Dvl forms many large cytoplasmic "puncta" per cell (11, 12, 14, 29). By contrast, at endogenous protein levels, we only observed 20 to 30% of cells with supramolecular Dvl2_mEos3.2 condensates in HEK293T cells (Fig. 2*A* and *SI Appendix*, Fig. S3*A*). A Dvl2_mEos3.2 expression construct designed analogously to our endogenously tagged HEK293T^{DVL2_mEos} cell line, however, showed the formation of numerous "puncta" (Fig. 2*A*), as previously reported (11, 12, 14, 29). This indicates that the amount of formed "puncta" depends on the amount of Dvl2 molecules which is highly increased upon overexpression.

To better understand the molecular nature of the condensates observed under physiological conditions and to rule out the possibility that the observed condensates represent unspecific aggregates of the mEos3.2 fluorophore, we confirmed the specificity of the mEos3.2 signal for Dvl2 by immunofluorescence stainings and confocal microscopy (Fig. 2*B*). The mEos3.2 colocalizes with the signal of a Dvl2-specific antibody in HEK293T^{DVL2_mEos} cells (Fig. 2*B*). We also excluded that the formation of condensates is solely driven by the attachment of the fluorophore. Accordingly, Dvl2 antibody stainings in wild-type HEK293T cells also showed supramolecular condensate formation resembling Dvl2_mEos3.2 condensates regarding size, distribution, and quantities (Fig. 2*C*). Dvl2 antibody stainings in DVL1,2,3^{KO} HEK293T and HEK293T^{DVL2_mEos} showed loss of the signal (*SI Appendix*, Fig. S3*B*). Together, these experiments indicate that the accumulation of Dvl2 in condensates is independent of tagging with the mEos3.2 fluorophore and that, in HEK293T wild-type cells at endogenous protein levels, Dvl2 condensate formation is limited to a subset of cells (Fig. 2 *A*–*C*).

Since Dvl is known to colocalize with Wnt signaling components upon overexpression (12, 23, 28, 63–65), we tested whether they can be found in endogenous condensates (Fig. 2*D*). Immunofluorescence stainings revealed that, also in endogenous condensates, Dvl2_mEos3.2 colocalizes with Dvl3, Axin1, and APC (Fig. 2*E*). Surprisingly, LRP6, a Wnt coreceptor, also localizes in these structures (Fig. 2*E*).

Next, we aimed to further characterize the endogenous condensates by investigating associated cellular structures. Endogenous supramolecular Dvl2_mEos3.2 condensates colocalized with neither markers for cell membranes (CellMask; *SI Appendix*, Fig. S2*C*) nor various proteins of the degradation machinery (see *SI Appendix*, Fig. S4 for lysosome [LAMP1], proteasome, ER and ER-associated degradation [Calnexin], and aggresomes [Vimentin]). These results indicate that Dvl2 condensates represent specific subunits of the cell, not colocalizing with known cellular structures, and that Dvl2 condensates are not primarily targeted for degradation.

Functional Validation of the HEK293T^{DVL2_mEos} Cell Line. To test the preserved functionality of the Dvl2 fusion protein in canonical Wnt signaling, responsiveness to Wnt signaling induction in HEK293T^{DVL2_mEos} cells was compared to the induction in HEK293T wild-type cells. Both cell lines were stimulated by the addition of recombinant Wnt3a (*SI Appendix*, Fig. S5*A*) or by overexpression of Wnt3 or Dvl2 (Fig. 3*A* and *SI Appendix*, Fig. S5*B*) to measure Wnt signaling activity using luciferase TCF4/Wnt reporter assays. HEK293T^{DVL2_mEos} cells showed no loss in responsiveness to Wnt activation.

In fact, we observed increased Wnt activity in the HEK293T^{DVL2_mEos} cells when compared to wild-type HEK293T

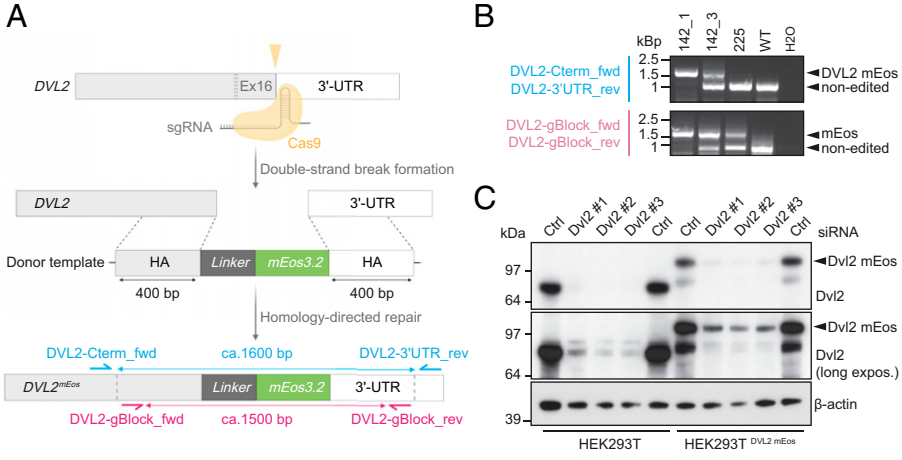

Fig. 1. Generation of endogenously tagged Dvl2_mEos3.2. (*A*) Schematic presentation of the knock-in design and tagging strategy. (*B*) Validation of the integration of the donor template into the *DVL2* locus. Genomic DNA was extracted from selected single-cell clones, and PCR was performed using the primers indicated in *A*. *Upper* shows correct integration into the *DVL2* locus (clones 142_1 and 142_3), whereas *Lower* reveals any integration in the genome (clone 225); kBp denotes kilobase pairs. (*C*) Dvl2_mEos3.2 protein expression in clone 142_3. The tagged protein is more abundant than nontagged Dvl2 in HEK293T^{DVL2_mEos}. Arrowheads indicate the endogenously mEos3.2-tagged Dvl2. Beta-actin serves as a loading control. One of three independent experiments is shown.

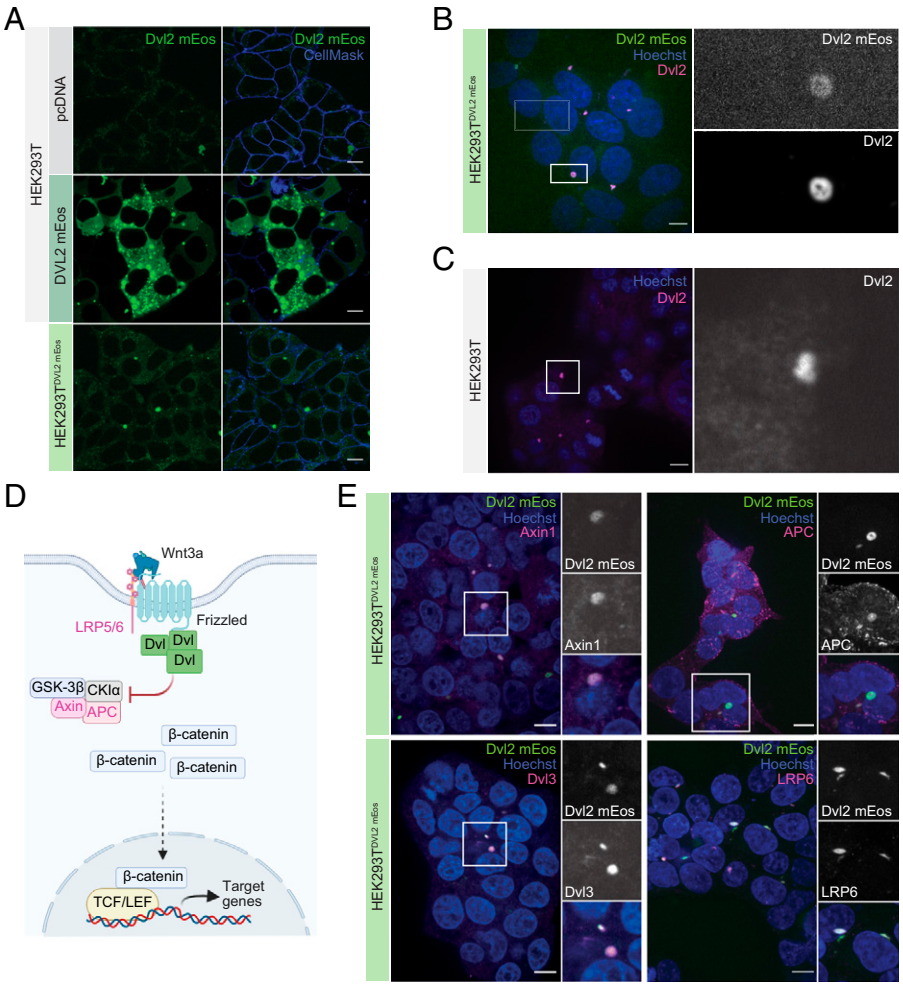

Fig. 2. Characterization of the endogenous Dvl2_mEos3.2 protein. (*A*) Correlative live-cell confocal microscopy of HEK293T^{DVL2_mEos} and HEK293T pcDNA DVL2_mEos3.2 shows that endogenous condensate formation is rare and limited to a subset of cells. The indicated HEK293T cells were transfected with pcDNA or pcDNA DVL2_mEos3.2 for 48 h. The same imaging settings were applied for all conditions, to enable the comparison of signal intensities of endogenous and overexpressed Dvl2_mEos3.2 protein. Green fluorescent signal in pcDNA is transfection-induced autofluorescence. In all confocal images, mEos3.2 is shown after excitation with 488 nm wavelength. Cell membrane was visualized using CellMask Deep Red membrane dye (blue). Representative images are of three replicates with imaging of three or more points of view. (Scale bar, 10 μm.) (*B* and *C*) Confocal microscopy of Dvl2 in HEK293T^{DVL2_mEos} (*B*) and wild-type (*C*) cells. Maximum intensity projections are shown of HEK293T^{DVL2_mEos} (z = 17) and wild type (z = 16). Representative images are of three or four replicates with imaging of three or more points of view. (Scale bar, 10 μm.) White boxes mark the magnified areas. (*D*) Current model of the activated beta-catenin–dependent Wnt signaling cascades. (*E*) Colocalization of Dvl3, Axin1, APC, and LRP6 with Dvl2_mEos3.2 in the condensates. Maximum intensity projections are shown of Dvl3 (z = 25), Axin1 (z = 26), APC (z = 25), and LRP6 (z = 15). Representative images are of three to five replicates with imaging of three or more points of view. (Scale bar, 10 μm.) White boxes mark the magnified areas.

cells. We suspected that, during single-cell isolation, a clone with enhanced capacity for Wnt signaling activation was selected. To rule out an effect of the mEos3.2-tag, we performed a knockout of mEos3.2 in the HEK293T^{DVL2_mEos} clone. Two mEos^{KO} pools, namely, mEos$^{KO2.1_I}$ and mEos$^{KO2.1_II}$, showed a strong reduction of Dvl2_mEos3.2 protein and an increase of wild-type Dvl2 protein. Still, both mEos^{KO} pools sustained enhanced signal strength in the TCF4/Wnt reporter assay (*SI Appendix*, Fig. S5 *C* and *D*). This indicates a clonality effect with increased responsiveness to Wnt signals independent of the addition of mEos3.2 to Dvl2 in HEK293T^{DVL2_mEos}.

To exclude compensatory mechanisms through other Dvl paralogs or modulated non-Dvl Wnt pathway components, we performed a double siRNA-mediated knockdown of both paralogs Dvl1 and Dvl3 (Fig. 3*B*). Dvl1 could still not be detected in HEK293T^{DVL2_mEos}. Both cell lines, HEK293T^{DVL2_mEos} and HEK293T, show equally reduced Wnt3 induction in the TCF4/Wnt reporter assay after Dvl1 and Dvl3 knockdown, arguing against compensatory functions of the other Dvl paralogs in the HEK293T^{DVL2_mEos} cell line (Fig. 3*C*).

To exclude compensatory functions of other Wnt signaling components, we performed CRISPR/Cas9-mediated DVL1,2,3^{KO} in both cell lines HEK293T^{DVL2_mEos} (pool) and HEK293T (clone; see also *SI Appendix*, Fig. S2 *B* and *C*). Both cell lines show correlatively reduced capability upon Wnt3 stimulation, while the TCF4/Wnt reporter activity can still be activated by the expression of beta-catenin (Fig. 3*D*). This result demonstrates that, apart from Dvl, no off-target or compensatory effects mediate TCF4 transcription in HEK293T^{DVL2_mEos} cells.

To test the preserved functionality of Dvl2_mEos3.2, we then investigated the recruitment of Dvl2_mEos3.2 to the plasma membrane after transient expression of different canonical and noncanonical Wnt receptors with and without Wnt stimulation. We generated fluorescently labeled expression constructs FZD7_tagRFP and ROR2_mScarlet and tested their activity. FZD7_tagRFP can restore Fzd function in mFZD^{KO} cells (57) to the same extent as nontagged Fzd7 as measured in the TCF4/Wnt reporter (*SI Appendix*, Fig. S6*A*). ROR2_mScarlet induces invasiveness of MCF7 breast cancer cells to the same extent as nontagged ROR2 (*SI Appendix*, Fig. S6*B*).

Overexpression of the canonical Wnt receptor Fzd7 and the noncanonical Wnt receptor ROR2 is sufficient to recruit Dvl2_mEos3.2 to the plasma membrane at endogenous Wnt levels (Fig. 3*E* for nontagged receptors; *SI Appendix*, Fig. S6*C* for tagged constructs). Overexpression of Wnt3a (FZD7_tagRFP) or Wnt5a (ROR2_mScarlet) did not lead to increased recruitment to the plasma membrane (*SI Appendix*, Fig. S6*C*).

Dvl2_mEos3.2 Condensate Formation in HEK293T Cells Depends on Wnt Signaling Upstream of Beta-Catenin. Since Dvl "puncta" were proposed to represent the activation of Wnt signaling ("signalosomes") (23), we tested the Wnt dependency of Dvl2_mEos3.2 condensates in HEK293T cells by modulating Wnt signaling at various levels. First, we coexpressed tagged and nontagged Wnt3a and Wnt5a constructs to activate canonical and noncanonical signaling pathways, respectively (*SI Appendix*, Fig. S7). Despite strong induction of the TCF4/Wnt reporter activity by Wnt3 (Fig. 3*A*), we could not observe

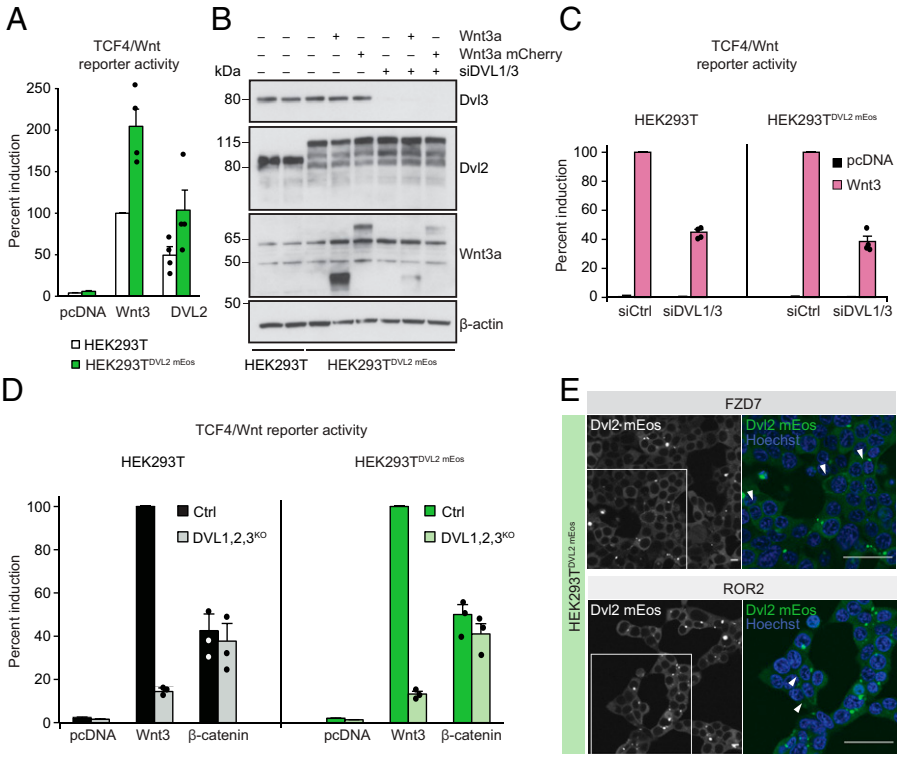

Fig. 3. Wnt activity is maintained in endogenously tagged Dvl2_mEos3.2 cells. (*A*) HEK293T^{DVL2_mEos} and HEK293T wild-type cells were transfected with pcDNA (empty vector control), Wnt3, and DVL2 together with TCF4/Wnt-firefly luciferase and actin-Renilla reporter plasmids. Induced reporter activity was determined by normalization to Wnt3 transfected HEK293T cells. Graph represents the mean ± SEM of four independent experiments. (*B* and *C*) Dvl1 and Dvl3 have no influence on the function of Dvl2_mEos3.2.HEK293T^{DVL2_mEos} and HEK293T wild-type cells were transfected with the indicated siRNAs against *DVL1/3,* or siCtl; 24 h later, cells were transfected with Wnt3a, Wnt3a_mCherry, or pcDNA; 48 h later, total cell lysates were collected and analyzed by Western blot. Note that Dvl1 is not expressed in HEK293T^{DVL2_mEos} and HEK293T cells (*SI Appendix*, Fig. S2*A*). One of three independent experiments is shown. Induced reporter activity was determined by normalization to HEK293T cells (siCtl.) stimulated with Wnt3. Graph represents the mean ± SEM of four independent experiments. (*D*) CRISPR/Cas9-mediated knockout of all Dvl paralogs (DVL1,2,3^{KO}) reduces Wnt3-driven TCF4/Wnt reporter activity in HEK293T^{DVL2_mEos} and HEK293T cells. Induced reporter activity was determined by normalization to Wnt3 transfected cells. Graph represents the mean ± SEM of three independent experiments. (*E*) Recruitment of Dvl2_mEos3.2 to the plasma membrane by overexpression of Fzd7 and ROR2. Live-cell confocal microscopy was performed with the same laser settings for all conditions. White boxes mark the magnified areas seen in the dual-color images. Arrowheads indicate membrane recruitment. DNA was stained by Hoechst (blue). Representative images are of three replicates with imaging of three or more points of view. (Scale bar, 10 μm; in magnifications, 25 μm.) For pcDNA control, see Fig. 4*E*.

apparent changes of condensate formation with confocal or widefield fluorescence microscopy by Wnt3a or Wnt5a overexpression (*SI Appendix*, Fig. S7). Again, we tested whether the presence of other Dvl paralogs would mask potential effects and performed siRNA-mediated knockdown of *DVL1* and *DVL3* in HEK293T^{DVL2_mEos}. No changes of Dvl2_mEos3.2 condensates or recruitment to the plasma membrane could be observed after coexpression of Wnt3a (Fig. 4*A*). Even though the receptor expression enhanced the recruitment of Dvl2_mEos3.2 to the plasma membrane, we could not detect differences in Dvl2_mEos3.2 condensates upon overexpression of Wnt3a or Wnt5a using confocal or widefield fluorescence microscopy. However, it could still be possible that basal Wnt signaling levels are sufficient for the presence of condensates in HEK293T cells.

We next inhibited basal Wnt signaling levels in the HEK293T^{DVL2_mEos} cells. We used two different single-guide RNAs (sgRNAs) to generate cell populations (pools) with knockout of *EVI/WLS,* a cargo receptor necessary for the secretion of Wnt proteins (66, 67). Loss of Evi and the lack of Wnt3 secretion were confirmed by Blue Sepharose pulldown and Western blot analysis (Fig. 4*B*). In line with these results, induction of the luciferase-based TCF4/Wnt reporter was inhibited after the expression of Wnt3 in EVI^{KO} cells but not upon beta-catenin expression, demonstrating the preserved transcriptional activity in all cell lines (Fig. 4*C*).

As we showed that the expression of Fzd7 and ROR2 leads to a relocalization of Dvl2_mEos3.2 to the plasma membrane independent of additional Wnt stimulus, we were interested in whether a reduced expression of receptors can influence the pattern of Dvl2_mEos3.2. To investigate this, we used HEK293T^{DVL2_mEos} cells with multiple knockouts of the predominantly expressed Frizzled receptors (Fzd 1, 2, 4, 5, 7, and 8 as published in ref. 57). As previously published, TCF4/Wnt reporter activity was absent in the HEK293T^{DVL2_mEos} mFZD^{KO} cell population (pool) after expression of Wnt3. However, expression of beta-catenin still induced luciferase signals (Fig. 4*D*).

For all three cell pools, we then investigated the formation of Dvl2_mEos3.2 condensates. Live-cell imaging revealed a reduction of Dvl2_mEos3.2 condensates in HEK293T^{DVL2_mEos} mFZD^{KO} and EVI^{KO} cells (representative images of mFZD^{KO} are shown in Fig. 4*E*). For an unbiased assessment, we performed an automated image analysis and quantification assay. Thus, we were able to detect significantly reduced numbers of cells with Dvl2_mEos3.2 condensates in the Wnt-inhibited cell lines, namely, HEK293T^{DVL2_mEos} EVI^{KOEX1_1} and EVI^{KOEX1_3} and HEK293T^{DVL2_mEos} mFZD^{KO} compared to HEK293T^{DVL2_mEos} control cells (Fig. 4*F*) (despite lower absolute counts of condensates in comparison to manual quantification [Fig. 4*F* and *SI Appendix*, Fig. S3*A*]).

To support the hypothesis that Dvl2_mEos3.2 condensate formation in HEK293T cells depends on active Wnt signaling, we performed a rescue experiment. Since EVI^{KOEX1_1} showed higher knockout efficiency (*SI Appendix*, Table S1) and lower condensate counts (Fig. 4*F*), we chose this EVI^{KO} pool and treated the cells with 200 ng/mL recombinant Wnt3a for 1, 3, or 16 h. Indeed, treatment with recombinant Wnt3a induced Dvl2 condensates starting 1 h after treatment and reaching approximately 90% after 16 h (Fig. 4*G*).

However, the treatment with recombinant Wnt3a in HEK293T^{DVL2_mEos} (Evi wt) cells did not significantly increase quantitative condensate counts detected with the automated assay (Fig. 4*G*), confirming previous observations by confocal live-cell microscopy with the expressed constructs. Even though both recombinant and expressed Wnt3(a) strongly induce transcriptional activity (see *SI Appendix*, Fig. S8*A* for TCF4/Wnt reporter assay), no changes in condensate counts could be detected (Fig. 4*G*).

Additionally, inhibition of transcriptional Wnt activity by siRNA-mediated knockdown of CTNNB1 (beta-catenin) had no

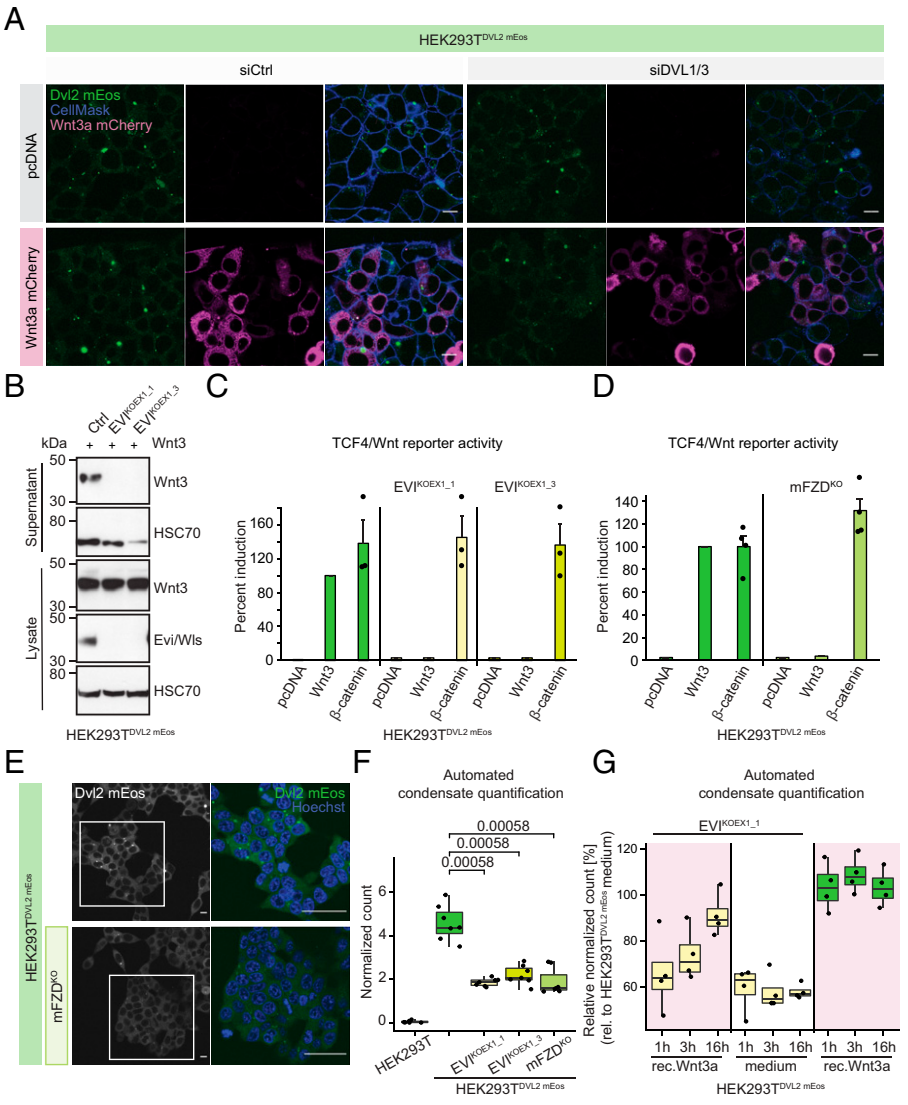

Fig. 4. Dvl2_mEos3.2 condensate formation depends on active Wnt signaling. (*A*) Knockdown of *DVL1/3* and additional Wnt stimulus have no impact on condensate formation. HEK293T^{DVL2_mEos} cells were transfected with siRNAs against *DVL1/3*; 24 h later, cells were transfected with the indicated siRNAs and plasmids (for transfection with Wnt5a_mScarlet, nontagged Wnt3a, and further controls, see *SI Appendix*, Fig. S7). Representative images are of four replicates with imaging of three or more points of view. (Scale bar, 10 μm.) (*B*) Expression of Evi/Wls protein and its secretion capacity in HEK293T^{DVL2_mEos} EVI^{KO} cells. Total cell lysates and Blue Sepharose enriched supernatants were used for Western blot analysis with the indicated antibodies. HSC70 serves as a loading control. One of three independent experiments is shown. (*C*) Canonical Wnt signaling is diminished in EVI^{KO} cells. Induced TCF4/Wnt-firefly luciferase reporter activity was determined by normalization to Wnt3 transfected HEK293T^{DVL2_mEos} cells. Graph represents the mean ± SEM of three independent experiments. (*D*) Canonical Wnt signaling is abolished in mFZD^{KO} cells. Graph represents the mean ± SEM of four independent experiments. (*E*) Loss of Wnt signaling due to mFZD^{KO} reduces condensate formation. Representative images are of three replicates with imaging of three or more points of view. (Scale bar, 10 μm; in magnifications, 25 μm.) White boxes mark the magnified areas seen in the dual-color images. Images show controls (pcDNA transfected) for Fig. 2*E*. (*F*) Knockout of *EVI* and *mFZD* significantly reduces Dvl2_mEos3.2 condensate formation. The condensate count was normalized to the number of cells per image (condensates per 100 cells). The quantification via automated image analysis detects less condensates compared to manual counting. Box plot represents the normalized condensate counts for the different cell lines, with dots representing the average normalized condensate count per plate (seven plates from three individual experiments). Statistical significance was calculated using the Wilcoxon signed rank test. (*G*) Stimulation with recombinant (rec.) Wnt3a induces Dvl2_mEos3.2 condensate formation in EVI^{KO} cells. The cells were treated either with murine rec. Wnt3a (final concentration 200 ng/mL; for activity of rec. Wnt3a, see *SI Appendix*, Fig. S8*A*) or medium (control). The automatically determined condensate count was normalized to the number of cells per image and related to the count of medium-treated HEK293T^{DVL2_mEos} cells of the same timepoint. Box plot is for the relative, normalized condensate counts, with dots representing the average relative, normalized condensate counts from four individual experiments.

quantitative effect on the number of condensates in the automated assay (*SI Appendix*, Fig. S8 *B* and *C*). This result indicates that Dvl2_mEos3.2 condensate formation is independent of Wnt-mediated transcriptional activity but governed upstream of Dvl2.

Dvl2_mEos3.2 Condensate Formation Is Cell Cycle Dependent. Previous studies have demonstrated that Wnt signaling and the cell cycle are closely intertwined (as reviewed in refs. 68–71). Several Wnt signaling components, such as Dvl, have been shown to play an active role during mitosis (72–75). Additionally, Wnt signaling seems to be differentially regulated at various cell cycle stages (76, 77). Interestingly, live-cell imaging revealed that, although interphase cells could be found with or without condensates, we never observed mitotic cells with Dvl2_mEos3.2 condensates (Fig. 5 *A* and *B*). We hypothesized that condensate formation is limited to only certain cell cycle stages and, more specifically, that condensate formation does not occur during mitosis.

To confirm and quantify our observation, we increased the number of mitotic cells by cell cycle synchronization using a double thymidine block. Eight to 10 h after cell cycle release, we observed the highest fraction of mitotic cells ("mitotic enrichment"), by Hoechst nuclear staining. However, even after the mitotic enrichment, we did not detect any condensate formation in mitotic cells (Fig. 5*B*). Together, these results indicate that condensate formation is impeded during mitosis, suggesting that the formation of Dvl2 condensates is cell cycle dependent. It confirms the close interplay of Wnt signaling and the cell cycle.

Dvl2_mEos3.2 Condensates Assemble at Gamma-Tubulin and CEP164-Positive Structures of the Centrosome. Previously, overexpressed Dvl2 was reported to be part of centrosomal structures (72, 73). Since we observed a cell cycle–dependent formation of Dvl2_mEos3.2 condensates in HEK293T cells, we analyzed whether endogenous Dvl2 condensates assemble at the centrosome.

We conducted stainings for gamma-tubulin and markers of the microtubule-organizing centers (MTOC)/pericentriolar material (PCM1) and confirmed that Dvl2_mEos3.2 localizes to condensates at the centrosomes (Fig. 5*C*). However, at endogenous protein levels, we did not observe accumulations of Dvl2_mEos3.2 at the spindle poles of cells undergoing mitosis, using confocal microscopy. Since nearly all Dvl2_mEos3.2 condensates formed at gamma-tubulin-positive structures but not all gamma-tubulin-positive structures showed Dvl2_mEos3.2 condensates, we speculate

that the accumulation of Dvl2_mEos3.2 at the centrosomes depends, at least in some part, on the cell and centrosome cycle.

Additionally, we observed that Dvl2_mEos3.2 polarized to one site of gamma-tubulin, suggesting that Dvl2 might localize specifically to the mother centriole. Another possible localization would be the basal bodies of cilia, which represent nonmitotic, gamma-tubulin structures and are a prominent place of Dvl localization and Wnt signaling integration hub (78–81). To investigate both hypotheses, we performed CEP164 stainings as a marker for the mother centriole and basal body. To visualize cilia, acetylated tubulin (AAT) was added. We performed confocal and structured illumination microscopy (SIM) which revealed that the endogenous Dvl2_mEos3.2 supramolecular condensates localized to the mother centriole but did not accumulate at the basal body in HEK293T ciliated cells (Fig. 5 *D* and *E*). Additionally, we gained the impression that the supramolecular condensates displayed substructuring (Fig. 5 *E*, *III*)

We did not observe condensates in cells with mature cilia, and thus hypothesized that cells in G_0 might also not form condensates. Nevertheless, reliable detection of single cilia in three-dimensional cells is challenging, and Wnt-dependent condensate formation in G_0 cannot be excluded.

SMLM to Analyze Dvl2_mEos3.2 Condensates. Recent technical advances made subdiffraction-limited imaging of cellular structures possible (51, 82–84).

Using PALM after integrating the mEos3.2 fluorophore into the *DVL2* locus (Fig. 6*A*), we demonstrate the feasibility of CRISPR PALM for single-molecule microscopy of context-regulated Wnt pathway components (Fig. 6*B*). CRISPR PALM reveals that the supramolecular Dvl2_mEos3.2 condensates are distinct structures with recurrent shapes, organization, and, indeed, substructures as suspected after performing SIM (Fig. 6*B*). Recurrent shapes include a shooting star–like lineup, C shapes, and round and donut-like shapes. Preserved and good photoconverting capacities of endogenous expression levels of mEos3.2 revealed repeating substructures within these shapes, that is, recurring patterning with smaller holes inside the larger shapes, especially when imaging Dvl2_mEos3.2 only (Fig. 6*B*; substructures are especially visible in the condensates labeled with "round").

To gain further insights into the composition of these supramolecular structures, substructuring, and their association with the CEP164-positive mother centriole, we combined PALM with another single-molecule localization technique: DNA-PAINT (Fig. 6*C*) (85). DNA-PAINT is an antibody-based

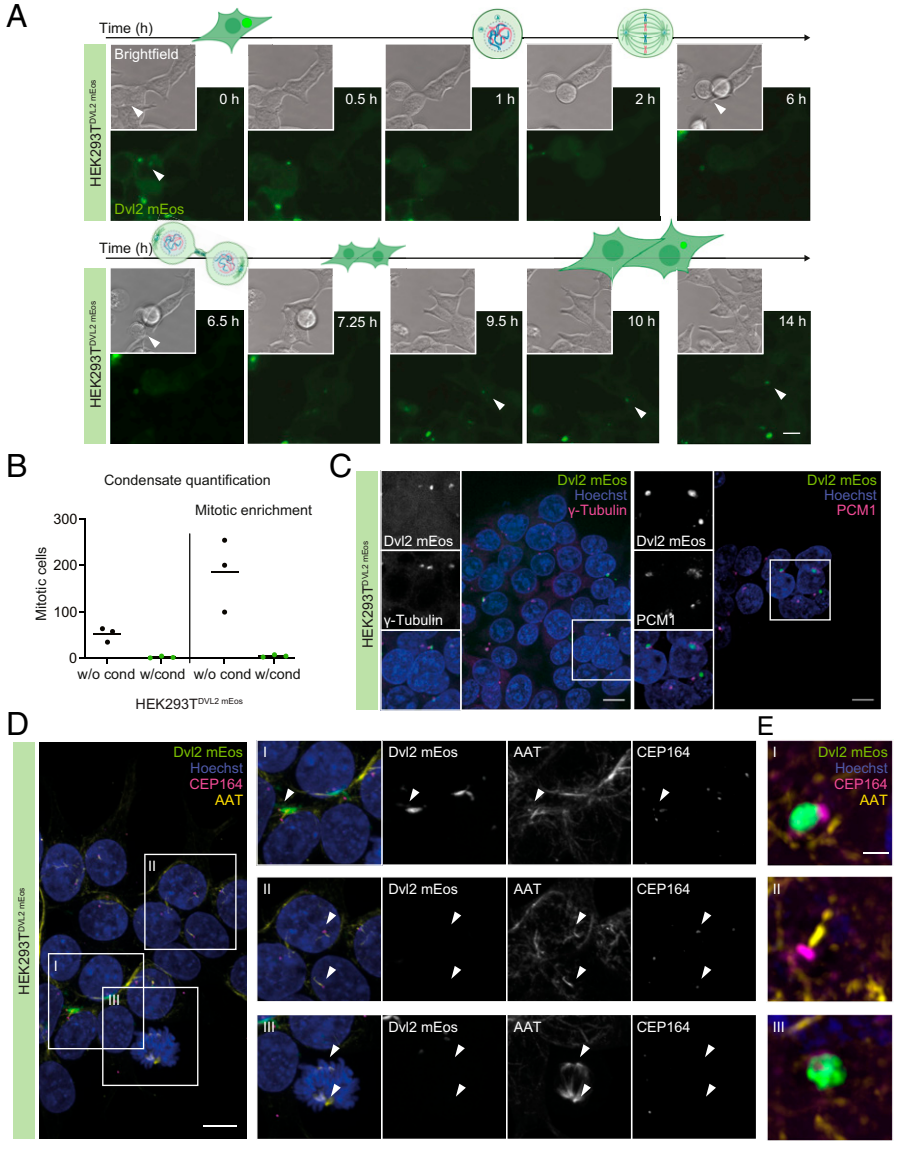

Fig. 5. Cell cycle–dependent localization of Dvl2_mEos3.2 condensates to the centrosome. (*A*) Exemplary time-lapse images are of two mitotic cells that lose condensates before and regain condensates after mitosis. At 0 h, two cells marked by arrowheads in bright-field and fluorescent images harbor condensates. After 1 h to 2 h, both cells enter mitosis. No fluorescent condensates can be observed. At time point 6.5 h, the first cell has started cytokinesis (marked by an arrowhead). At 9.5 h, cell division is completed, and a new condensate starts forming (arrowheads in 9.5, 10, and 14 h). The images were taken on an A1 Nikon microscope every 15 min for 15 h under physiological conditions. Maximum intensity projections of four slices spanning a total of 3 μm are shown. (Scale bar, 10 μm.) See also Movie S1. (*B*) Formation of Dvl2_mEos3.2 condensates is inhibited in mitotic cells. For enrichment of mitotic cells, HEK293T^{DVL2_mEos} cells were synchronized by double thymidine block. Manual counting was done of mitotic cells with and without Dvl2_mEos3.2 condensates in four fields-of-view per experiment (20× magnification). Bar represents the mean of three independent experiments that are shown by dots. (*C*) Dvl2_mEos3.2 condensates localize to the pericentriolar matrix/centrosome in HEK293T^{DVL2_mEos} cells. Confocal microscopy is of HEK293T^{DVL2_mEos} cells with gamma-tubulin or PCM1 antibodies (magenta). Maximum intensity projections are shown of gamma-tubulin (z = 21) and PCM1 (z = 31). Representative images of three or four replicates with imaging of five or more points of view. (Scale bar, 10 μm.) White boxes mark the magnified areas. (*D*) Dvl2_mEos3.2 condensates localize to the mother centriole in interphase cells. HEK293T^{DVL2_mEos} cells were stained with the centrosomal marker CEP164 (magenta) and AAT (yellow). *I*–*III* represent magnifications as indicated by white boxes of (*I*) mother centriole, (*II*) basal body of cilia, and (*III*) spindle poles. Maximum intensity projections are shown (z = 30). Representative images of four replicates with imaging of six or more points of view. (Scale bar, 10 μm.) (*E*) SIM confirms Dvl2_mEos3.2 condensates at the centrioles (*I*), lack of condensate formation at cilia (*II*), and revealed distinct substructures (*III*). Multiple Z planes were acquired with 200 nm distance. Maximum intensity projections are shown (z = 7). (Scale bar, 1 μm.)

imaging method, where the secondary antibody is labeled with DNA oligonucleotides (also called target or "docking" strands). Imaging is performed after the addition of dye-labeled oligonucleotides ("imager" strands). Transient binding of the imager to the docking strands creates the mandatory blinking to detect single molecules (85) (Fig. 6*C*).

Even though mEos3.2 showed better photoconversion capacities revealing more substructures when imaged in D_2O for CRISPR PALM (Fig. 6*B*), photoconversion of mEos3.2 was still good when imaging in the DNA-PAINT imaging buffer (Fig. 6*D*). The costaining with CEP164-DNA-PAINT-atto655 revealed that the donut-like Dvl2_mEos3.2 structure was usually found to enclose a singular CEP164 mother centriole (Fig. 6*D*). When two CEP164-positive ring structures were observed by SMLM, as reported before the release of the distal appendage proteins from the two mature mother centrioles prior to mitosis (86), Dvl2_mEos3.2 was instead found next to the two centrioles in a C-like shape (Fig. 6*D*). However, when we observed the shooting star–like structure of mEos3.2, a single centriole could be found polarized to one end of the alignment, like a fireball followed by the Dvl2_mEos3.2 tail (Fig. 6*D*). These results indicate that the association of Dvl2_mEos3.2 in HEK293T cells is dynamic and changes during the cell and centrosomal cycle.

Surprisingly, the Dvl2_mEos3.2 condensates in HEK293T cells also contained varying amounts of CEP164 (Fig. 6*D*). These observations lead to intriguing speculations on the role of Dvl2 condensates in the assembly and disassembly of centrosomal structures. We observed proliferative deficits in DVL1,2,3^{KO} cells in a live-cell assay after 2 d compared to the wild-type counterpart (*SI Appendix*, Fig. S9). However, qualitative deficiencies still need to be investigated in more detail.

Discussion

Here, we show that Dvl2 localizes to distinct, supramolecular, membraneless structures at endogenous protein levels and under physiological regulation in HEK293T cells. These structures form dynamically in a Wnt- and Dvl2 concentration-dependent manner. Their formation appears to be rather decoupled from transcriptional activity downstream of beta-catenin. Additionally, Dvl at endogenous levels colocalizes in

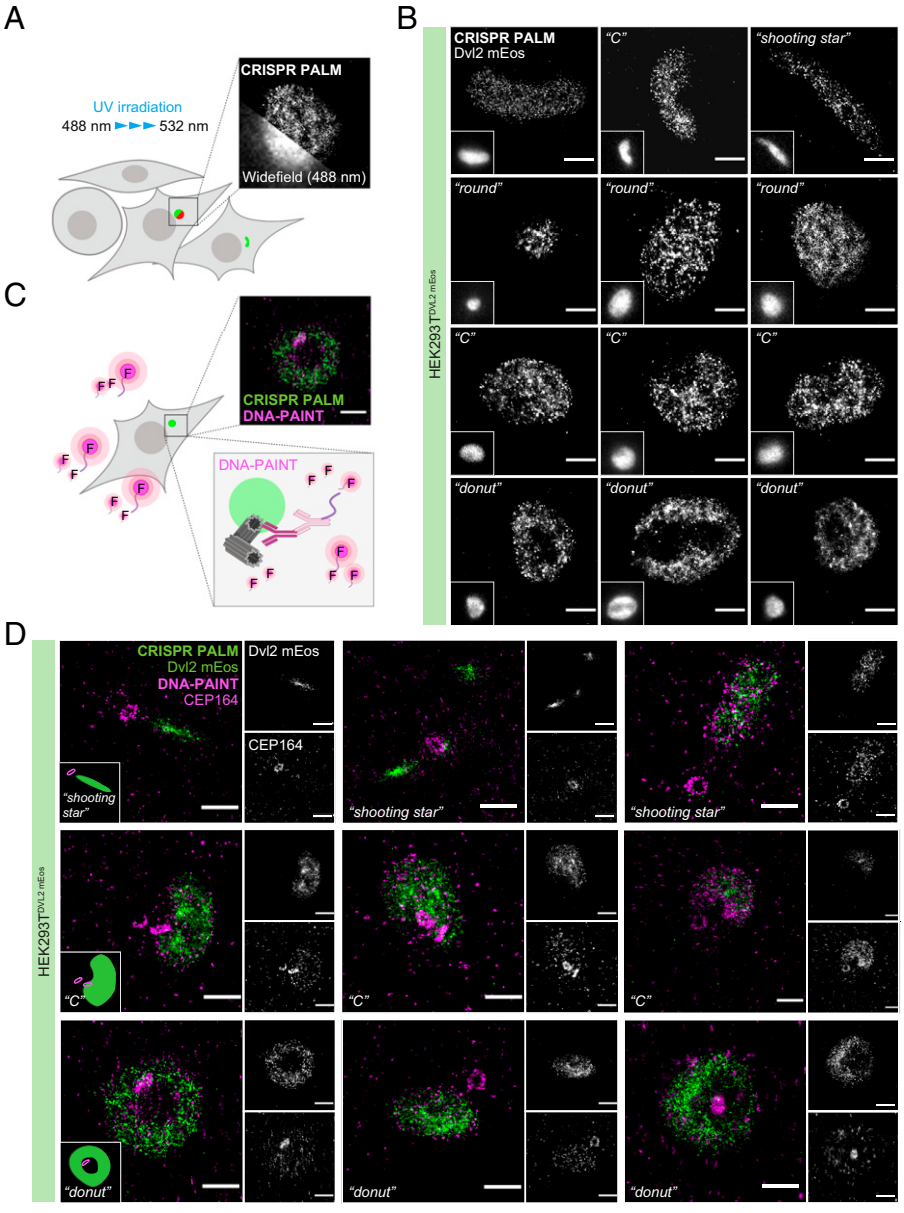

Fig. 6. SMLM reveals repetitive shapes of Dvl2_mEos3.2 condensates at various stages of the centrosomal cycle. (*A*) Model of UV irradiation-induced photoconversion of mEos3.2 for CRISPR PALM including representative images of *B*. (*B*) Endogenous Dvl2_mEos3.2 unravels supramolecular condensates with distinct shapes and substructures in HEK293T^{DVL2_mEos} cells. Recurrent shapes include a shooting star–like lineup, C shapes, and round and donut-like shapes. Substructures within these shapes, that is, recurring patterning with smaller holes inside the larger shapes, are especially visible in the condensates labeled with "round." *Insets* show widefield images of the respective condensate. Representative images of SMLM of ≥30 condensates are shown. (Scale bar, 1 μm.) (*C*) Model of dual-color image acquisition using CRISPR PALM in combination with DNA-PAINT including a representative image of *D*. (*D*) Repetitive shapes of Dvl2_mEos3.2 condensates in relation to the mother centriole. Dual-color, single-molecule microscopy was performed in HEK293T^{DVL2_mEos} cells using CRISPR PALM (mEos; green) in combination with DNA-PAINT (CEP164; magenta). *Insets* are schematic pictograms showing the spatial relation of the mother centriole and the respective Dvl2_mEos3.2 condensate shape. Representative images of SMLM of ≥60 condensates are shown. (Scale bar, 1 μm.)

these structures with other Wnt signaling components, such as Dvl3, Axin1, and APC (43, 46). We analyze Dvl supramolecular condensates by combining CRISPR gene editing with PALM and DNA-PAINT superresolution imaging technologies. We demonstrate a cell cycle dependency of the Wnt-dependent condensates which can be formed in interphase cells at the centrosome. The Wnt-dependent colocalization of these condensates with components of centrosomes highlights the close interplay of Wnt signaling and the cell cycle.

Biomolecular condensates have been proposed as membraneless organelles mediating the correct proceedings of various physiological reactions (34). The characteristics of biomolecular condensates include their dynamic formation by phase separation of, for example, proteins through specialized domains, a free exchange of molecules, and a size that can reach up to multiple micrometers (34, 35). We show, in HEK293T cells at endogenous protein levels, that Dvl2 forms non-membrane-bound, multiple micrometers spanning intracellular substructures containing, most likely, hundreds of Dvl2 molecules. There, multiple other Wnt signaling components such as Dvl3, Axin1, LRP6, APC, and, most likely, other Wnt-(un)related proteins are localized. Like Dvl2, Dvl3, Axin1, and APC are scaffolding proteins, and some of them have been shown to undergo LLPS in vitro through their IDRs (42, 43). Other proteins of these complexes would qualify as corecruited clients, for example, CEP164. We demonstrate that these structures do not represent cellular garbage recycling or degradation compartments such as lysosomes, proteasomes, or aggresomes. Contextual change, such as the inhibition of Wnt signaling upstream of Dvl, inhibits the recruitment of Dvl2 to these large, dynamic structures suggesting Wnt-dependent compartmentalization to fulfill a specific—yet not further specified—cellular function. That the recruitment of Dvl2 into the complex is dynamic but appears to be saturable at a level where transcriptional activity can still be induced hints toward a tightly controlled process. Based on current definitions of biomolecular condensates as dynamic, non-membrane-bound organelles that form through LLPS (34, 35, 41, 87), we conclude that these large endogenous multiprotein complexes represent biomolecular condensates.

Another striking observation was the presence of the transmembrane protein LRP6 in the membrane-less Wnt-dependent condensates. Previous studies showed a strong membrane localization of LRP6 in HEK293T cells, but, in these studies, overexpression constructs were used (23, 88–92). By contrast, a recent study with endogenously mCherry-labeled LRP6 in NCI-H1703 cells indicated only faint membrane localization but a strong signal in the perinuclear region (89). Similarly, we did not observe membrane localization of endogenous LRP6, presumably due to the selected image settings for the detection of the much brighter cytoplasmic condensates.

The specific LRP6 antibody (e.g., ref. 93) recognizes the amino acid residues enclosing Met-1409 of human LRP6, that is, the C-terminal and cytoplasmic receptor section. LRP6 is an LDLR. As for other members of the receptor family (e.g., Notch, APP, and ErbB4), it was suggested that LRP6 is subjected to gamma-secretase-dependent regulated intramembrane proteolysis (94). The work of Mi and Johnson (94) indicates a protein kinase C, Wnt3a/DKK1 regulated process, where the extracellular receptor domain is cast off into the surroundings, and the cytoplasmic end is shed through gamma-secretase-like activity. They also show that the intracellular domain (ICD) then associates with GSK3, thereby activating Wnt signaling. The importance of stable polymerization of Dvl and LRP6 for cytoplasmic "signalosome" formation was further highlighted by Metcalfe et al. (95). Here, overexpression of a DVL–DIX:LRP6–ICD chimera lacking the LRP6 transmembrane domain promoted Wnt/beta-catenin signaling through the induction of cytoplasmic "signalosomes." The signaling-active chimera was also found in membraneless "puncta" not colocalizing with caveolin or other endocytic vesicle markers. Taken together, colocalization of the LRP6 antibody signal with other Wnt signaling components in the membraneless Dvl2_mEos3.2 condensates could, in fact, support the hypotheses of Mi and Johnson as well as Metcalf et al.: after Wnt signaling activation the LRP6–ICD is cleaved and associates with Dvl in biomolecular condensates. Nevertheless, additional experiments are necessary to further support this hypothesis.

We demonstrate that, at endogenous protein levels, Dvl condensate formation is observed in 20 to 30% of HEK293T cells and is limited to, usually, one supramolecular condensate per cell that accumulates at the CEP164-positive end of the interphase centrosome, thus in close proximity to the mother centriole. SMLM revealed that the CEP164-positive mother centriole can be found enclosed in a donut-like Dvl2_mEos3.2 shape and that CEP164 can be found occasionally in the pericentrosomal condensates. Besides the above-mentioned role of Dvl as a crucial signaling integration hub in Wnt signaling, Dvl and various other Wnt signaling components have been demonstrated to control cell and centrosomal cycle, cell division, and functions of cilia. Dvl, when expressed at low levels, has been described to colocalize with centrosomal structures to regulate mitotic progression (72) and ciliary disassembly (80), to support the removal of centrosomal linker proteins (73) and the planar polarization of the basal body in ciliated cells (78). Additionally, various Dvl-phosphorylating kinases regulate mitotic progression, for example, PLK1 (72), NEK2 (58, 73), and Aurora A (58). However, centrosome-orchestrated events such as cell cycle regulation by Wnt signaling and the role of Dvl in this context remain a largely uninvestigated field, especially at physiological and cell state-corresponding protein levels.

Interestingly, Dvl2_mEos3.2 supramolecular condensates were not detected at the CEP164-positive basal body of full-grown cilia. However, this does not exclude a function of Dvl2 in the assembly or disassembly of cilia (80). In contrast to a previous study, our data indicate that Dvl2 supramolecular condensates do not colocalize with the midbody or spindle poles in mitosis in HEK293T cells (72).

Centrosomes represent MTOC necessary for assembling the mitotic spindle, cell polarity, and asymmetric cell division. They also have been described as non-membrane-bound compartments containing two centrioles in the PCM which is dynamically assembled and disassembled. Hereby centrosomes also mimic condensate-like features (96). In interphase, only a thin PCM base coat of ∼200 nm is established. During the preparation for mitosis, a less-organized PCM layer forms that can reach multiple micrometers (96). Various scaffolding proteins have been described to self-assemble and take part in establishing this PCM compartment (96). It is therefore reasonable that, while the composition of the PCM changes during the course of the cell cycle, Wnt signaling components are more or less likely to associate with these structures.

Wnt signaling and the cell cycle are tightly linked, and several models have been proposed regarding the role of Dvl in this context: 1) The centrosome acts as an interaction hub for Wnt signaling: The vicinity of various pathway components could create the optimal environment for adequate signal transmission (as reviewed in refs. 71 and 97). 2) Wnt signaling components instead regulate the localization and composition of

centrosomal proteins and the proper centrosome cycle, for example, by modulating centrosomal splitting and mitotic progression (72–74, 98–102). The observed proximity of Dvl2 and other Wnt signaling components such as Dvl3, Axin1, APC, and LRP6 makes the first model an intriguing concept, which, in the end, does not rule out that those components also have functional relevance for the centrosome. NEK2 has been described to phosphorylate Dvl (73). Additionally, NEK2 was shown to remove distal appendage proteins such as CEP164 from the mother centriole at G2/M before cells enter mitosis (86). The proximity of mature CEP164 centriolar pairs with the cup-like condensates (most likely at G2/M), enclosure of the single mother centriole by the Dvl2_mEos3.2 donut (most likely earlier, e.g., in interphase), and the fact that Dvl2_mEos3.2 condensates contain additional, non-distal-appendage CEP164 proteins, and that DVL1,2,3^{KO} reduces cell proliferation trigger further speculations about Dvl's role for proper mitotic progression in HEK293T cells.

During the generation and functional analysis of the HEK293T^{DVL2_mEos} cell line, it was surprising that Dvl2 condensate formation was limited to a subset of cells and usually one large structure per cell. This result is consistent with Ma et al. (49) and Kan et al. (27), who recently published their endogenously tagged cell lines focusing on membrane dynamics of Dvl and reported similar observations of a low number of "puncta." The absence of the previously described numerous "puncta'' and the lack of change of quantities and distribution after Wnt stimulation raised the question of whether a C-terminally tagged fusion protein, per se, may not be entirely functional (103, 104). For example, a C-terminally attached protein could limit the ability of Dvl2 to change into its "closed" conformation where the Dvl C terminus is proposed to directly interact with its PDZ domain (103, 104). The resulting somewhat "open" conformation of Dvl2 might activate JNK more effectively when compared to nontagged Dvl2 (103, 104). Additionally, a modified capability for membrane localization and receptor binding was discussed (103). However, our data demonstrate the preserved functionality of the Dvl2 fusion protein and its responsiveness to various kinds of Wnt signaling modifications such as receptor expression levels and amount of Wnt ligand stimulus. Moreover, the recruitment of Dvl2_mEos3.2 to the plasma membrane by the canonical and noncanonical receptors Fzd7 and ROR2 was not impaired. Various knockout and knock-in constellations also exclude compensatory mechanisms of other Dvl paralogs in the HEK293T^{DVL2_mEos} cell line, emphasizing that critical functional analysis of gene fusion products is a crucial step of quality control after CRISPR/Cas-mediated gene editing.

In line with our results, Ma et al. (49) and Kan et al. (27) detected few large "puncta" that appeared to be stable and not responsive to Wnt3a stimulus. Similarly, we did not observe changes in condensate formation in HEK293T^{DVL2_mEos} cells after stimulation with recombinant Wnt3a or the expression of various Wnt constructs. While Ma et al. used Wnt signaling "reduction" conditions (short-term LGK974 treatment), they showed structurally similar condensates as observed in our study under native conditions. Through efficient inhibition of Wnt signaling upstream of Dvl, namely, CRISPR-mediated mFZD^{KO} and EVI^{KO}, we could demonstrate Wnt dependency of Dvl2 supramolecular condensate formation in HEK293T cells. In addition, Dvl2_mEos3.2 condensate formation was induced in EVI^{KO} cells using recombinant Wnt3a. Although the automated condensate quantification assay might underestimate the absolute amounts of Dvl2_mEos3.2 condensates, it is a powerful assay to detect significant numerical changes. It could be that minor quantitative and, especially, qualitative condensate changes as, for example, observed by TIRF at the plasma membrane (27, 49) remain undetected due to the applied imaging or quantification method. Also, the assay does not enable the detection of differences in condensate size. In line with Ma et al., we observed membrane recruitment by expression of Fzd, yet no membrane localization of Dvl2 after Wnt stimulation. It needs to be noted that the formation of very small Dvl2 membrane "puncta" was only detected by TIRF, not by confocal microscopy (27, 49).

Even though we can demonstrate that Dvl2_mEos3.2 supramolecular condensates form in a dynamic and Wnt-dependent manner, and rather decoupled from transcriptional activity downstream of beta-catenin, we can only speculate what saturates their formation. It could be that activated Dvl2 can only associate with the centrosome at certain cell cycle stages; therefore, only a certain percentage of cells are capable of harboring these supramolecular condensates. These might further increase in size with additional Wnt stimulus, which remained undetected in our assays. Additionally, it is possible that the amounts of other condensate components, scaffolds such as APC and Axin1, or the activity of certain kinases are limiting factors implicating that Dvl polymers are less stable than associations with other scaffolds. Constitutively expressed Dvl2 forms multiple cytoplasmic supramolecular condensates in HEK293T cells. However, increased Wnt stimulus was not sufficient to induce multiple condensates per cell, raising questions on the roles of protein amounts, phosphorylation status, and qualitative differences of endogenous vs. overexpression condensates.

By monitoring various Wnt signaling components expressed at near-endogenous levels in the *Drosophila* embryo, Schaefer et al. (105) were able to observe a supramolecular assembly of various "destruction complex" components. In their study, Axin was recruited to the plasma membrane, and *Drosophila* Dvl was additionally recruited to the complex in Wnt-ON cells (105). Our experimental setup did not enable us to examine whether the formation of the Dvl2-containing condensates took place at the plasma membrane. Since HEK293T cells have a small cytoplasm-to-nucleus ratio, membraneless perinuclear/pericentrosomal condensates can still be in close proximity to the outer plasma membrane. Nevertheless, it is noteworthy that we observed Axin1 and APC condensates that did not harbor Dvl2_mEos3.2. Further experiments are necessary, for example, through Axin1 fluorescent labeling or knockout variants of APC and Axin in the HEK293T^{DVL2_mEos} cells, to determine the dependency of Dvl2 condensate formation on the presence and localization of these other scaffolding proteins.

But what are the functions of Dvl2 condensates? It has been controversial for quite some time whether "puncta" are necessary for Wnt signaling transmission (e.g., refs. 14 and 29). While we show that Wnt3a is able to induce—to a certain extent—Dvl2 supramolecular condensate formation in HEK293T cells, transcriptional activity can further be promoted, while condensates appear quantitatively stable. Also, mitotic HEK293T cells lack supramolecular Dvl2 condensates, while others have shown that cells in M phase are capable of Wnt signaling (76, 77). This suggests that Wnt signaling can be active in the absence of large supramolecular condensates. Potential further functions of the supramolecular condensates that need to be determined include condensates as highly regulated storage pools that increase—to a certain extent—with upstream Wnt signals, or a mechanism of turning off (low-threshold) signals.

We propose a model where, depending on the cellular context (e.g., active Wnt signaling), concentration, and phosphorylation

status, Dvl2 polymerizes and localizes to supramolecular condensates in HEK293T cells. At endogenous protein levels and certain cell cycle stages, the PCM appears to present the optimal environment to host these Wnt signaling condensates. Nevertheless, when overexpressed and taken out of the physiological cellular context, Dvl and other Wnt signaling components can condense at other cellular localizations. SIM of the overexpressed scaffolding proteins Axin-RFP/GFP-APC2 in SW480 cells shows quantitative differences compared to our results but shows a condensate architecture structurally similar to our endogenous Dvl2_mEos3.2 condensates observed using SIM and CRISPR PALM (e.g., donut-like shapes, subcompartmentalization) (65, 105). We suggest that these large, multiprotein condensates represent a hub for the dynamic interaction of various Wnt signaling components such as kinases and scaffolds that mediate the prompt redirection of signaling outcomes in a fine-tuned, concentration-dependent manner. The model is in line with findings that APC and Dvl compete for the interaction with Axin (63, 65, 106). They propose that it can occur in the same subcellular compartment, likely considering the fine architecture of condensates and the distinct arrangement of Dvl2 molecules examined in this study, allowing the formation of further subcompartments.

Nevertheless, intriguing questions remain: 1) whether periodic changes in Wnt signaling activity during the cell cycle reach the critical concentrations, compositions, or valency for the formation of multiprotein condensates in only specific cell cycle stages or 2) whether changes in the composition of the PCM will only allow for the accumulation of phosphorylated Dvl after Wnt activation in and as part of the then more complex PCM. Further experiments will define the exact role of the scaffolding protein Dvl2 and endogenous Dvl2 condensates at the centrosome and their context-dependent regulation.

Materials and Methods

Detailed information on materials and methods can be found in *SI Appendix, SI Materials and Methods*.

For endogenous tagging, sgRNAs targeting human *DVL2* at its C terminus or the beginning of the 3′-untranslated region (UTR) were designed using the E-CRISP web service and cloned into the PX459 vector (107). A gBlock (synthesized by IDT) served as a homology-directed repair template. Fluorescent single-cell clones were validated by PCR, Sanger sequencing (Eurofins Genomics), and Western blot. Multitargeting sgRNAs for *DVL1,2,3* were generated and characterized by nested PCR and MiSeq Next Generation Sequencing as previously reported (57) (*SI Appendix*, Table S1). For automated condensate quantification, intensity-based thresholding and region growing identified individual nuclei and cell bodies based on the DNA and F-actin staining. Condensates were then determined inside regions covered by cells. For PALM imaging of mEos3.2 only, cells were imaged in phosphate-buffered saline prepared containing 90% D_2O and 10% H_2O. DNA-PAINT was used according to the manufacturer's instructions (Massive-AB 1-Plex DNA-PAINT kit anti-mouse atto655, Massive Photonics). For two-color imaging with PALM and DNA-PAINT, mEos3.2 was sequentially imaged after the DNA-PAINT acquisition without buffer exchange.

Data Availability. All study data are included in the article and/or supporting information. Code is provided through GitHub (108).

ACKNOWLEDGMENTS. We thank K. Löffler and M. Weidmann for their technical support. We thank F. Heigwer, L. Wolf, F. Port, and all members of the M.B. laboratory for helpful discussions. We thank the teams of the Nikon Imaging Center at Heidelberg University and the Advanced Light Microscopy Facility at the European Molecular Biology Laboratory. We thank S. Takada, B. Kurtulmus, G. Pereira, S. P. Acebron, and A. Krämer for providing reagents. Figures were, in part, created with BioRender. A.S. received financial support from the University Medical Center Göttingen through the "Kolleg für Translationale Medizin" and the "Clinician Scientist Program" of the German Cancer Research Center (DKFZ) supported by the Dieter Morszeck Foundation. A.S. is a fellow of the "School of Oncology" of the Deutsches Konsortium für Translationale Krebsforschung (DKTK). This work was, in part, supported by Deutsche Forschungsgemeinschaft (DFG) SFB1324, "Mechanisms and Functions of Wnt signaling" (Project 331351713).

Author affiliations: [a]Division of Signaling and Functional Genomics, German Cancer Research Center and Department of Cell and Molecular Biology, Heidelberg University and BioQuant, 69120 Heidelberg, Germany; [b]Department of Hematology and Medical Oncology, University Medical Center Göttingen, 37075 Göttingen, Germany; [c]Department of Medical Oncology, National Center for Tumor Diseases, University Hospital Heidelberg, 69120 Heidelberg, Germany; [d]Advanced Light Microscopy Facility, European Molecular Biology Laboratory, 69117 Heidelberg, Germany; and [e]Nikon Imaging Center, BioQuant and Centre for Organismal Studies, Heidelberg University, 69120 Heidelberg, Germany

Author contributions: A.S., O.V., L.T., C.B., U.E., and M.B. designed research; A.S., O.V., F.R., P.G., C.S., T.M., M.S., M.L., and U.E. performed research; A.S., O.V., F.R., P.G., C.S., and U.E. contributed new reagents/analytic tools; A.S., O.V., F.R., P.G., C.S., M.L., and U.E. analyzed data; and A.S., D.K., and M.B. wrote the paper.

Competing interest statement: M.B. received research grants from Cellzome/GSK and Merck/Darmstadt unrelated to this study.

1. H. Clevers, R. Nusse, Wnt/β-catenin signaling and disease. *Cell* **149**, 1192–1205 (2012).
2. T. Zhan, N. Rindtorff, M. Boutros, Wnt signaling in cancer. *Oncogene* **36**, 1461–1473 (2017).
3. Z. Zhong, J. Yu, D. M. Virshup, B. Madan, Wnts and the hallmarks of cancer. *Cancer Metastasis Rev.* **39**, 625–645 (2020).
4. M. Boutros, M. Mlodzik, Dishevelled: At the crossroads of divergent intracellular signaling pathways. *Mech. Dev.* **83**, 27–37 (1999).
5. J. B. Wallingford, R. Habas, The developmental biology of Dishevelled: An enigmatic protein governing cell fate and cell polarity. *Development* **132**, 4421–4436 (2005).
6. P. Paclíková *et al.*, Roles of individual human Dishevelled paralogs in the Wnt signalling pathways. *Cell. Signal.* **85**, 110058 (2021).
7. M. Gentzel, A. Schambony, Dishevelled paralogs in vertebrate development: Redundant or distinct? *Front. Cell Dev. Biol.* **5**, 59 (2017).
8. M. Boutros, N. Paricio, D. I. Strutt, M. Mlodzik, Dishevelled activates JNK and discriminates between JNK pathways in planar polarity and wingless signaling. *Cell* **94**, 109–118 (1998).
9. M. Sharma, I. Castro-Piedras, G. E. Simmons, K. Pruitt, Dishevelled: A masterful conductor of complex Wnt signals. *Cell. Signal.* **47**, 52–64 (2018).
10. N. Perrimon, A. P. Mahowald, Multiple functions of segment polarity genes in *Drosophila*. *Dev. Biol.* **119**, 587–600 (1987).
11. F. Fagotto *et al.*, Domains of Axin involved in protein-protein interactions, Wnt pathway inhibition, and intracellular localization. *J. Cell Biol.* **145**, 741–756 (1999).
12. M. J. Smalley *et al.*, Interaction of Axin and Dvl-2 proteins regulates Dvl-2-stimulated TCF-dependent transcription. *EMBO J.* **18**, 2823–2835 (1999).
13. D. G. S. Capelluto *et al.*, The DIX domain targets Dishevelled to actin stress fibres and vesicular membranes. *Nature* **419**, 726–729 (2002).
14. T. Schwarz-Romond, C. Merrifield, B. J. Nichols, M. Bienz, The Wnt signalling effector Dishevelled forms dynamic protein assemblies rather than stable associations with cytoplasmic vesicles. *J. Cell Sci.* **118**, 5269–5277 (2005).
15. C. P. Ponting, C. Phillips, K. E. Davies, D. J. Blake, PDZ domains: Targeting signalling molecules to sub-membranous sites. *BioEssays* **19**, 469–479 (1997).
16. B. N. R. Cheyette *et al.*, Dapper, a Dishevelled-associated antagonist of beta-catenin and JNK signaling, is required for notochord formation. *Dev. Cell* **2**, 449–461 (2002).
17. H.-C. Wong *et al.*, Direct binding of the PDZ domain of Dishevelled to a conserved internal sequence in the C-terminal region of Frizzled. *Mol. Cell* **12**, 1251–1260 (2003).
18. W. J. Pan *et al.*, Characterization of function of three domains in Dishevelled-1: DEP domain is responsible for membrane translocation of Dishevelled-1. *Cell Res.* **14**, 324–330 (2004).
19. D. V. F. Tauriello *et al.*, Wnt/β-catenin signaling requires interaction of the Dishevelled DEP domain and C terminus with a discontinuous motif in Frizzled. *Proc. Natl. Acad. Sci. U.S.A.* **109**, E812–E820 (2012).
20. J. D. Axelrod, J. R. Miller, J. M. Shulman, R. T. Moon, N. Perrimon, Differential recruitment of Dishevelled provides signaling specificity in the planar cell polarity and Wingless signaling pathways. *Genes Dev.* **12**, 2610–2622 (1998).
21. M. Boutros, J. Mihaly, T. Bouwmeester, M. Mlodzik, Signaling specificity by Frizzled receptors in *Drosophila*. *Science* **288**, 1825–1828 (2000).
22. F. Cong, L. Schweizer, H. Varmus, Casein kinase Iepsilon modulates the signaling specificities of Dishevelled. *Mol. Cell. Biol.* **24**, 2000–2011 (2004).
23. J. Bilic *et al.*, Wnt induces LRP6 signalosomes and promotes Dishevelled-dependent LRP6 phosphorylation. *Science* **316**, 1619–1622 (2007).
24. J. M. Peters, R. M. McKay, J. P. McKay, J. M. Graff, Casein kinase I transduces Wnt signals. *Nature* **401**, 345–350 (1999).
25. V. Bryja, G. Schulte, N. Rawal, A. Grahn, E. Arenas, Wnt-5a induces Dishevelled phosphorylation and dopaminergic differentiation via a CK1-dependent mechanism. *J. Cell Sci.* **120**, 586–595 (2007).
26. M. V. Gammons, M. Renko, C. M. Johnson, T. J. Rutherford, M. Bienz, Wnt signalosome assembly by DEP domain swapping of Dishevelled. *Mol. Cell* **64**, 92–104 (2016).
27. W. Kan *et al.*, Limited Dishevelled/Axin oligomerization determines efficiency of Wnt/β-catenin signal transduction. *eLife* **9**, e55015 (2020).
28. T. Schwarz-Romond, C. Metcalfe, M. Bienz, Dynamic recruitment of Axin by Dishevelled protein assemblies. *J. Cell Sci.* **120**, 2402–2412 (2007).
29. M. J. Smalley *et al.*, Dishevelled (Dvl-2) activates canonical Wnt signalling in the absence of cytoplasmic puncta. *J. Cell Sci.* **118**, 5279–5289 (2005).
30. M. A. Julius *et al.*, Domains of Axin and disheveled required for interaction and function in Wnt signaling. *Biochem. Biophys. Res. Commun.* **276**, 1162–1169 (2000).

31. S. Kishida *et al.*, DIX domains of Dvl and Axin are necessary for protein interactions and their ability to regulate beta-catenin stability. *Mol. Cell. Biol.* **19**, 4414–4422 (1999).
32. T. Schwarz-Romond *et al.*, The DIX domain of Dishevelled confers Wnt signaling by dynamic polymerization. *Nat. Struct. Mol. Biol.* **14**, 484–492 (2007).
33. X. Zeng *et al.*, Initiation of Wnt signaling: Control of Wnt coreceptor Lrp6 phosphorylation/activation via frizzled, Dishevelled and Axin functions. *Development* **135**, 367–375 (2008).
34. S. F. Banani, H. O. Lee, A. A. Hyman, M. K. Rosen, Biomolecular condensates: Organizers of cellular biochemistry. *Nat. Rev. Mol. Cell Biol.* **18**, 285–298 (2017).
35. K. N. Schaefer, M. Peifer, Wnt/Beta-catenin signaling regulation and a role for biomolecular condensates. *Dev. Cell* **48**, 429–444 (2019).
36. A. S. Lyon, W. B. Peeples, M. K. Rosen, A framework for understanding the functions of biomolecular condensates across scales. *Nat. Rev. Mol. Cell Biol.* **22**, 215–235 (2021).
37. P. J. Flory, Thermodynamics of high polymer solutions. *J. Chem. Phys.* **10**, 51–61 (1942).
38. S. F. Banani *et al.*, Compositional control of phase-separated cellular bodies. *Cell* **166**, 651–663 (2016).
39. C. P. Brangwynne, P. Tompa, R. V. Pappu, Polymer physics of intracellular phase transitions. *Nat. Phys.* **11**, 899–904 (2015).
40. C. W. Pak *et al.*, Sequence determinants of intracellular phase separation by complex coacervation of a disordered protein. *Mol. Cell* **63**, 72–85 (2016).
41. M. Bienz, Head-to-tail polymerization in the assembly of biomolecular condensates. *Cell* **182**, 799–811 (2020).
42. T.-M. Li *et al.*, Multivalent tumor suppressor adenomatous polyposis coli promotes Axin biomolecular condensate formation and efficient β-catenin degradation. *Sci. Rep.* **10**, 17425 (2020).
43. J. Nong *et al.*, Phase separation of Axin organizes the β-catenin destruction complex. *J. Cell Biol.* **220**, e202012112 (2021).
44. M. Gammons, M. Bienz, Multiprotein complexes governing Wnt signal transduction. *Curr. Opin. Cell Biol.* **51**, 42–49 (2018).
45. M. C. Faux *et al.*, Recruitment of adenomatous polyposis coli and β-catenin to Axin-puncta. *Oncogene* **27**, 5808–5820 (2008).
46. Q. Shi, K. Kang, Y.-G. Chen, Liquid-liquid phase separation drives the β-catenin destruction complex formation. *BioEssays* **43**, e2100138 (2021).
47. S. M. de Man, G. Zwanenburg, T. van der Wal, M. A. Hink, R. van Amerongen, Quantitative live-cell imaging and computational modeling shed new light on endogenous WNT/CTNNB1 signaling dynamics. *eLife* **10**, e66440 (2021).
48. G. Ambrosi *et al.*, Allele-specific endogenous tagging and quantitative analysis of β-catenin in colorectal cancer cells. *eLife* **11**, e64498 (2022).
49. W. Ma *et al.*, Single-molecule dynamics of Dishevelled at the plasma membrane and Wnt pathway activation. *Proc. Natl. Acad. Sci. U. S. A.* **117**, 166690–16701 (2020).
50. M. Sauer, M. Heilemann, Single-molecule localization microscopy in Eukaryotes. *Chem. Rev.* **117**, 7478–7509 (2017).
51. E. Betzig *et al.*, Imaging intracellular fluorescent proteins at nanometer resolution. *Science* **313**, 1642–1645 (2006).
52. A. O. Khan *et al.*, Optimised insert design for improved single-molecule imaging and quantification through CRISPR-Cas9 mediated knock-in. *Sci. Rep.* **9**, 14219 (2019).
53. A. O. Khan, V. A. Simms, J. A. Pike, S. G. Thomas, N. V. Morgan, CRISPR-Cas9 mediated labelling allows for single molecule imaging and resolution. *Sci. Rep.* **7**, 8450 (2017).
54. W.-K. Cho *et al.*, Super-resolution imaging of fluorescently labeled, endogenous RNA Polymerase II in living cells with CRISPR/Cas9-mediated gene editing. *Sci. Rep.* **6**, 35949 (2016).
55. M. Zhang *et al.*, Rational design of true monomeric and bright photoactivatable fluorescent proteins. *Nat. Methods* **9**, 727–729 (2012).
56. N. Durisic, L. Laparra-Cuervo, A. Sandoval-Álvarez, J. S. Borbely, M. Lakadamyali, Single-molecule evaluation of fluorescent protein photoactivation efficiency using an in vivo nanotemplate. *Nat. Methods* **11**, 156–162 (2014).
57. O. Voloshanenko, P. Gmach, J. Winter, D. Kranz, M. Boutros, Mapping of Wnt-Frizzled interactions by multiplex CRISPR targeting of receptor gene families. *FASEB J.* **31**, 4832–4844 (2017).
58. K. Hanáková *et al.*, Comparative phosphorylation map of Dishevelled 3 links phospho-signatures to biological outputs. *Cell Commun. Signal.* **17**, 170 (2019).
59. B. Del Valle-Pérez, O. Arqués, M. Vinyoles, A. G. de Herreros, M. Duñach, Coordinated action of CK1 isoforms in canonical Wnt signaling. *Mol. Cell. Biol.* **31**, 2877–2888 (2011).
60. V. Bryja, L. Cajánek, A. Grahn, G. Schulte, Inhibition of endocytosis blocks Wnt signalling to β-catenin by promoting Dishevelled degradation. *Acta Physiol. (Oxf.)* **190**, 55–61 (2007).
61. O. Bernatik *et al.*, Sequential activation and inactivation of Dishevelled in the Wnt/β-catenin pathway by casein kinases. *J. Biol. Chem.* **286**, 10396–10410 (2011).
62. Y.-N. Lee, Y. Gao, H.-Y. Wang, Differential mediation of the Wnt canonical pathway by mammalian Dishevelleds-1, -2, and -3. *Cell. Signal.* **20**, 443–452 (2008).
63. C. Mendoza-Topaz, J. Mieszczanek, M. Bienz, The Adenomatous polyposis coli tumour suppressor is essential for Axin complex assembly and function and opposes Axin's interaction with Dishevelled. *Open Biol.* **1**, 110013 (2011).
64. M. B. C. Kilander *et al.*, Disheveled regulates precoupling of heterotrimeric G proteins to Frizzled 6. *FASEB J.* **28**, 2293–2305 (2014).
65. K. N. Schaefer *et al.*, Wnt regulation: Exploring Axin-Disheveled interactions and defining mechanisms by which the SCF E3 ubiquitin ligase is recruited to the destruction complex. *Mol. Biol. Cell* **31**, 992–1014 (2020).
66. K. Bartscherer, N. Pelte, D. Ingelfinger, M. Boutros, Secretion of Wnt ligands requires Evi, a conserved transmembrane protein. *Cell* **125**, 523–533 (2006).
67. I. Augustin *et al.*, Loss of epidermal Evi/Wls results in a phenotype resembling psoriasiform dermatitis. *J. Exp. Med.* **210**, 1761–1777 (2013).
68. C. Niehrs, S. P. Acebron, Mitotic and mitogenic Wnt signalling. *EMBO J.* **31**, 2705–2713 (2012).
69. A. Stolz, H. Bastians, Fresh WNT into the regulation of mitosis. *Cell Cycle* **14**, 2566–2570 (2015).
70. P. Kaldis, M. Pagano, Wnt signaling in mitosis. *Dev. Cell* **17**, 749–750 (2009).
71. V. Bryja, I. Červenka, L. Čajánek, The connections of Wnt pathway components with cell cycle and centrosome: Side effects or a hidden logic? *Crit. Rev. Biochem. Mol. Biol.* **52**, 614–637 (2017).
72. K. Kikuchi, Y. Niikura, K. Kitagawa, A. Kikuchi, Dishevelled, a Wnt signalling component, is involved in mitotic progression in cooperation with Plk1. *EMBO J.* **29**, 3470–3483 (2010).
73. I. Cervenka *et al.*, Dishevelled is a NEK2 kinase substrate controlling dynamics of centrosomal linker proteins. *Proc. Natl. Acad. Sci. U.S.A.* **113**, 9304–9309 (2016).
74. Y. E. Greer, J. S. Rubin, Casein kinase 1 delta functions at the centrosome to mediate Wnt-3a-dependent neurite outgrowth. *J. Cell Biol.* **192**, 993–1004 (2011).
75. D. S. Sepich, M. Usmani, S. Pawlicki, L. Solnica-Krezel, Wnt/PCP signaling controls intracellular position of MTOCs during gastrulation convergence and extension movements. *Development* **138**, 543–552 (2011).
76. G. Davidson *et al.*, Cell cycle control of Wnt receptor activation. *Dev. Cell* **17**, 788–799 (2009).
77. S. P. Acebron, E. Karaulanov, B. S. Berger, Y.-L. Huang, C. Niehrs, Mitotic Wnt signaling promotes protein stabilization and regulates cell size. *Mol. Cell* **54**, 663–674 (2014).
78. T. J. Park, B. J. Mitchell, P. B. Abitua, C. Kintner, J. B. Wallingford, Dishevelled controls apical docking and planar polarization of basal bodies in ciliated epithelial cells. *Nat. Genet.* **40**, 871–879 (2008).
79. E. K. Vladar, J. D. Axelrod, Dishevelled links basal body docking and orientation in ciliated epithelial cells. *Trends Cell Biol.* **18**, 517–520 (2008).
80. K. H. Lee *et al.*, Identification of a novel Wnt5a-CK1ε-Dvl2-Plk1-mediated primary cilia disassembly pathway. *EMBO J.* **31**, 3104–3117 (2012).
81. Y. Zilber *et al.*, The PCP effector Fuzzy controls cilial assembly and signaling by recruiting Rab8 and Dishevelled to the primary cilium. *Mol. Biol. Cell* **24**, 555–565 (2013).
82. M. J. Rust, M. Bates, X. Zhuang, Sub-diffraction-limit imaging by stochastic optical reconstruction microscopy (STORM). *Nat. Methods* **3**, 793–795 (2006).
83. S. T. Hess, T. P. K. Girirajan, M. D. Mason, Ultra-high resolution imaging by fluorescence photoactivation localization microscopy. *Biophys. J.* **91**, 4258–4272 (2006).
84. K. I. Willig, S. O. Rizzoli, V. Westphal, R. Jahn, S. W. Hell, STED microscopy reveals that synaptotagmin remains clustered after synaptic vesicle exocytosis. *Nature* **440**, 935–939 (2006).
85. J. Schnitzbauer, M. T. Strauss, T. Schlichthaerle, F. Schueder, R. Jungmann, Super-resolution microscopy with DNA-PAINT. *Nat. Protoc.* **12**, 1198–1228 (2017).
86. L. Viol *et al.*, Nek2 kinase displaces distal appendages from the mother centriole prior to mitosis. *J. Cell Biol.* **219**, e201907136 (2020).
87. A. Boija, I. A. Klein, R. A. Young, Biomolecular condensates and cancer. *Cancer Cell* **39**, 174–192 (2021).
88. H. Sakane, H. Yamamoto, A. Kikuchi, LRP6 is internalized by Dkk1 to suppress its phosphorylation in the lipid raft and is recycled for reuse. *J. Cell Sci.* **123**, 360–368 (2010).
89. A. F. Eckert *et al.*, Measuring ligand-cell surface receptor affinities with axial line-scanning fluorescence correlation spectroscopy. *eLife* **9**, e55286 (2020).
90. G. Colozza *et al.*, Wnt-inducible Lrp6-APEX2 interacting proteins identify ESCRT machinery and Trk-fused gene as components of the Wnt signaling pathway. *Sci. Rep.* **10**, 21555 (2020).
91. M. E. Binnerts *et al.*, The first propeller domain of LRP6 regulates sensitivity to DKK1. *Mol. Biol. Cell* **20**, 3552–3560 (2009).
92. H. Yamamoto, H. Sakane, H. Yamamoto, T. Michiue, A. Kikuchi, Wnt3a and Dkk1 regulate distinct internalization pathways of LRP6 to tune the activation of beta-catenin signaling. *Dev. Cell* **15**, 37–48 (2008).
93. N. Giebel *et al.*, USP42 protects ZNRF3/RNF43 from R-spondin-dependent clearance and inhibits Wnt signalling. *EMBO Rep.* **22**, e51415 (2021).
94. K. Mi, G. V. W. Johnson, Regulated proteolytic processing of LRP6 results in release of its intracellular domain. *J. Neurochem.* **101**, 517–529 (2007).
95. C. Metcalfe, C. Mendoza-Topaz, J. Mieszczanek, M. Bienz, Stability elements in the LRP6 cytoplasmic tail confer efficient signalling upon DIX-dependent polymerization. *J. Cell Sci.* **123**, 1588–1599 (2010).
96. J. B. Woodruff *et al.*, The centrosome is a selective condensate that nucleates microtubules by concentrating tubulin. *Cell* **169**, 1066–1077.e10 (2017).
97. C. Arquint, A.-M. Gabryjonczyk, E. A. Nigg, Centrosomes as signalling centres. *Philos. Trans. R. Soc. Lond. B Biol. Sci.* **369**, 20130464 (2014).
98. S. Bahmanyar *et al.*, β-catenin is a Nek2 substrate involved in centrosome separation. *Genes Dev.* **22**, 91–105 (2008).
99. K. Fumoto, M. Kadono, N. Izumi, A. Kikuchi, Axin localizes to the centrosome and is involved in microtubule nucleation. *EMBO Rep.* **10**, 606–613 (2009).
100. B. C. Mbom, K. A. Siemers, M. A. Ostrowski, W. J. Nelson, A. I. M. Barth, Nek2 phosphorylates and stabilizes β-catenin at mitotic centrosomes downstream of Plk1. *Mol. Biol. Cell* **25**, 977–991 (2014).
101. Q. J. He *et al.*, Secreted Wnt6 mediates diabetes-associated centrosome amplification via its receptor FZD4. *Am. J. Physiol. Cell Physiol.* **318**, C48–C62 (2020).
102. A. T. Weiner *et al.*, Endosomal Wnt signaling proteins control microtubule nucleation in dendrites. *PLoS Biol.* **18**, e3000647 (2020).
103. J. Qi *et al.*, Autoinhibition of Dishevelled protein regulated by its extreme C terminus plays a distinct role in Wnt/β-catenin and Wnt/planar cell polarity (PCP) signaling pathways. *J. Biol. Chem.* **292**, 5898–5908 (2017).
104. H.-J. Lee, D.-L. Shi, J. J. Zheng, Conformational change of Dishevelled plays a key regulatory role in the Wnt signaling pathways. *eLife* **4**, e08142 (2015).
105. K. N. Schaefer *et al.*, Supramolecular assembly of the beta-catenin destruction complex and the effect of Wnt signaling on its localization, molecular size, and activity in vivo. *PLoS Genet.* **14**, e1007339 (2018).
106. M. I. Pronobis, N. M. Rusan, M. Peifer, A novel GSK3-regulated APC:Axin interaction regulates Wnt signaling by driving a catalytic cycle of efficient βcatenin destruction. *eLife* **4**, e08022 (2015).
107. F. Heigwer, G. Kerr, M. Boutros, E-CRISP: Fast CRISPR target site identification. *Nat. Methods* **11**, 122–123 (2014).
108. A. Schubert, Supp_Schubert_2021. GitHub. https://github.com/boutroslab/Supp_Schubert_2021. Deposited 23 June 2022.